Antigen binding by conformational selection in near-germline antibodies

Ryan J. Blackler[1] , Sven Müller-Loennies[2] , Barbara Pokorny-Lehrer[3] , Max S. G. Legg[1] , Lore Brade[2],
Helmut Brade[2], Paul Kosma[3] , and Stephen V. Evans[1],*

From the [1]Department of Biochemistry and Microbiology, University of Victoria, Victoria British Columbia, Canada; [2]Research Center Borstel, Leibniz Lung Center, Borstel, Germany; [3]Department of Chemistry, University of Natural Resources and Life Sciences, Vienna, Austria

Edited by Chris Whitfield

Conformational flexibility in antibody-combining sites has been hypothesized to facilitate polyspecificity toward multiple unique epitopes and enable the limited germline repertoire to match an overwhelming diversity of potential antigens; however, elucidating the mechanisms of antigen recognition by flexible antibodies has been understandably challenging. Here, multiple liganded and unliganded crystal structures of the near-germline anticarbohydrate antibodies S25–2 and S25–39 are reported, which reveal an unprecedented diversity of complementarity-determining region H3 conformations in apparent equilibrium. These structures demonstrate that at least some germline or near-germline antibodies are flexible entities sensitive to their chemical environments, with conformational selection available as an evolved mechanism that preserves the inherited ability to recognize common pathogens while remaining adaptable to new threats.

The human immune system produces a limited repertoire of germline antibodies that must recognize, ideally, every potential antigen. Germline antibody diversity is generated during the recombination of Variable (V), Diversity (D), and Joining (J) gene segments (1), which may yield over 10^{13} unique antibodies that are limited by the approximately 10^{11} B cells in circulation at a given time (2). Despite the enormity of this repertoire, it is ultimately finite, so at least some antibodies must be able to recognize many different antigens to protect against the almost limitless potential for antigenic diversity in the environment (3).

The ability of a single antibody to bind to multiple chemically distinct antigens, termed "polyspecificity" (4), may occur through structural flexibility of the antibody-binding site to generate multiple unique paratopes (5–8). Although the mechanism of antigen recognition by flexible antibodies is often attributed to "induced fit" (IF), where an initial weak interaction is followed by a structural rearrangement to improve complementarity, there has been a paradigm shift in the last decade to view proteins as complex conformational ensembles where binding can occur through "conformational selection" (CS) (9–12). Despite a surge in evidence for CS in protein–ligand binding in general, there have been relatively few discussions of CS as a mechanism of antigen binding by antibodies (8, 13–21), which is at odds with the profound importance of flexibility in antigen recognition for germline antibody diversity, autoimmunity, and allergy (22) and in structure prediction for antibody engineering (23).

Here we present a targeted structural investigation into the conformational equilibrium and antigen binding potential of two near-germline antibodies, S25–2 and S25–39. These antibodies were raised against *Chlamydiaceae* lipopolysaccharide oligosaccharides of 3-deoxy-α-D-*manno*-oct-2-ulopyranosonic acid (Kdo; Fig. 1)—a conserved carbohydrate component also in many other Gram-negative bacteria—and descend from the same germline gene segments, with four and six amino acid mutations, respectively (Table S1) (24). They have an almost identical complementarity-determining region (CDR) H3 (^{95}DHDGYYERFA/SY^{102}, where S25–2 has Ser H101 and S25–39 has Ala H101) that had been observed previously in three unique unliganded conformations as well as a single shared liganded conformation that is cross-reactive for several natural and unnatural Kdo oligosaccharides (Fig. S1, *A–E*) (24–27).

To investigate further the potential paratope diversity of these antibodies, the structures of their antigen-binding fragments (Fabs) were determined from crystals grown in dozens of novel conditions both unliganded and in the presence of antigens designed to complement some of the observed unliganded paratopes.

Results

Crystal structure of S25–39 in complex with 4-MeO-KdoAll

The crystal structure of S25–39 in complex with 4-MeO-KdoOAll was solved to 2.00 Å resolution in space group $P2_1$ with one molecule in the asymmetric unit (AU). The structure displays excellent electron density for all main chain atoms, with the exception of residues H127 to H133 in the constant region (the opposite end of the Fab from the combining site) that are disordered and not modeled. Data collection and refinement statistics are given in Table S2.
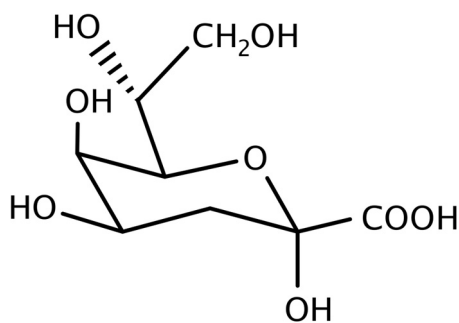
Figure 1. Chemical structure of 3-deoxy-α-D-*manno*-oct-2-ulopyranosonic acid (Kdo). The sugar 3-deoxy-α-D-*manno*-oct-2-ulopyranosonic acid is a characteristic carbohydrate component found in LPS oligosaccharides from Chlamydiaceae and many other Gram-negative bacteria. LPS, lipopolysaccharide.

The backbone of CDR H3 adopts the same conformation as in previous structures of S25–39 in complex with Kdo antigens, but with an important difference: the Glu H100A (numbered according to Kabat scheme (28)) side chain is completely disordered and neighboring CDR H3 residues have elevated B-factors relative to the average B-factor of the structure (Fig. S1, *F* and *G*). Despite Glu H100A side chain disorder, the 4-MeO-KdoOAll antigen exhibits complete electron density within the antibody-combining site in a 2Fo-Fc map contoured at 1σ, and with only atom C5 in the hexose ring displaying a lack of density in an omit map contoured at 2σ (Fig. S1, *G–I*), as do the remaining modeled residues of CDR H3 (Fig. S2A).

Crystal structures of S25–39 grown with synthetic antigens

Following the structural characterization of S25–39 in complex with 4-MeO-KdoOAll, we synthesized further Kdo-derived synthetic antigens, 4-O-benzyl-KdoOMe, 4-O-ethoxymethyl-KdoOMe, and 4-O-methoxymethyl-KdoOMe (Figs. S3–S12), and crystallized these with both S25–2 and S25–39.

Three unique and unliganded S25–39 structures were solved from crystals grown in the presence of these antigens. Two of these structures were solved in space group P2₁ (Unliganded #1 and Unliganded #2, to 1.53-Å and 1.30-Å resolution, respectively, each with one molecule in the AU) and one in space group C2 (Unliganded #3, to 2.10 Å with four molecules in the AU). Data collection and refinement statistics are given in Table S2.

Unliganded #1 (grown in the presence of 4-O-methoxymethyl-KdoOMe) displays excellent electron density for all main chain atoms, with the exception of residues H127 to H133 in the constant region that are disordered and not modeled. Electron density for a BIS-TRIS molecule from crystallization buffer was observed to be coordinated to Glu H148, Val H150, and Ala H168 in the constant region. This structure shows a nearly identical CDR H3 conformation to the original (27) unliganded S25–39 structure but was solved to significantly higher resolution (Fig. S2B). No electron density corresponding to ligand is observed.

Unliganded #2 (grown in the presence of 4-O-methoxymethyl-KdoOMe) displays excellent electron density for all main chain atoms, with the exception of residues H127 to H133 that are disordered and not modeled. The CDR H3 backbone adopts a nearly identical conformation to that observed in previous structures of S25–39 in complex with Kdo antigens and was solved to significantly higher resolution (Fig. S2C). No electron density corresponding to ligand is observed.

Unliganded #3 (grown in the presence of 4-O-ethoxymethyl-KdoOMe) displays good electron density for all main chain atoms, with the exception of residues H100B in CDR H3 of chain H, H127 to H134, B100A to B100B in CDR H3 of chain B, B127 to B132, D127 to D133, F98 to F100B in CDR H3 of chain F, and F127 to F133, which are disordered and not modeled. The four molecules in the AU include two unique conformations of CDR H3 in molecules H and D and two partially disordered conformations in B and F (Fig. S2, *D–G*). In one out of the four molecules in the AU (light/heavy chains labeled C/D) there was ambiguous electron density in the antigen-binding site where 4-O-ethoxymethyl-KdoOMe could have been modeled (Fig. S13). This density, however, could be equally well modeled by water molecules, and the omit difference map is more consistent with water molecules, so waters were included in the final structure. Binding data were not collected to evaluate this interaction. No electron density corresponding to ligand is observed for any of the remaining three molecules in the AU.

Crystal structures of S25–2 grown with synthetic antigens

Two unique and unliganded S25–2 structures were solved from crystals grown in the presence of 4-O-methoxymethyl-KdoOMe. No well-diffracting crystals were obtained from conditions containing 4-O-ethoxymethyl-KdoOMe. The conformations of the unliganded structures of S25–2 reported here, Unliganded #3 and Unliganded #4 (Unliganded #1 and #2 of S25–2 correspond to previously published (25) structures 1Q9K and 1Q9L, respectively), were both solved in space group P2₁ to 2.15-Å and 2.0-Å resolution, respectively, each with four molecules in the AU. Data collection and refinement statistics are given Table S2.

Unliganded #3 displays good electron density for all main chain atoms, with the exception of residues B100B and B100C of CDR H3 of chain B, B128 to B133, and D127 to D133, which are disordered and not modeled. The four molecules in the AU display three unique conformations of CDR H3, with one conformation occurring twice, one conformation partially disordered (Fig. S2, *H–K*), and all conformations different from the previously observed S25–2 Unliganded #1 and Unliganded #2. All antigen-binding sites include several interactions with a symmetry-related Fab molecule, including a salt bridge between the binding site Arg 52 of the heavy chain and Glu 213 of the symmetry-related light chain, mimicking the salt bridge to the carboxylate of Kdo antigens. No electron density corresponding to ligand is observed. Each Fab in the AU makes slightly different contacts to the symmetry-related molecules in the binding sites.

Unliganded #4 displays good electron density for all main chain atoms with the exception of H98 to H100A of CDR H3 in molecule H, and F128 to F133, which are disordered and not modeled. This crystal was grown in 0.2 M ammonium iodide, and 34 iodide ions are modeled in the final structure. Three out of four molecules in the AU display an identical CDR H3 conformation that is different from those previously observed, and the fourth is partially disordered (Fig. S2, L–O). Each CDR H3 coordinates three iodide ions in similar positions (Fig. S14). The structure displays the same crystal packing as Unliganded #3 described earlier, with a symmetry-related molecule occupying each binding site. No electron density corresponding to ligand is observed. None of the four Fab molecules of Unliganded #4 shows further structural differences from other S25–2 structures due to iodide coordination.

Discussion

Synthetic antigens can shift conformational equilibrium

The activity of unique paratopes generated through conformation flexibility was investigated by structure-based ligand design. In the first determined structures of S25–2 and S25–39 in complex with Kdo oligosaccharides (25, 27), a single Kdo residue is bound in a germline pocket with CDR H3 in a "kinked" conformation* (28, 29), where Glu H100A forms a bidentate interaction with Kdo O4 (Fig. S1A). In contrast, the first determined unliganded structures revealed an extended CDR H3 where Glu H100A is rotated away from the binding site, resulting in an expansion of a pocket around Kdo O4 when the ligand is superimposed (Fig. S1A) (25, 27). Modified Kdo ligands with 4-O-methyl, 4-O-benzyl, 4-O-ethoxymethyl, and 4-O-methoxymethyl substituents were synthesized to explore the antigen binding potential of this expanded pocket and alternate CDR H3 conformations (Figs. S3–S12).

In the crystal structure of S25–39 in complex with 4-O-methyl-KdoOAll, antigen is observed in the combining site with CDR H3 in the well-characterized Kdo-liganded conformation but with Glu H100A disordered and B-factors elevated for the remainder of CDR H3 (Fig. S1, F–I), indicating that this backbone conformation is still favorable even in the absence of the important Glu H100A interaction. Maintenance of binding to 4-O-methyl-KdoOAll despite the disruption of the important hydrogen bond to Glu H100A and concomitant destabilization of CDR H3 emphasizes the versatility of this V-gene–conserved Kdo-binding pocket that has previously been shown to cross-react with alternate lengths, linkages, and unnatural modifications of Kdo oligosaccharides through a single binding site conformation (24).

Structures were also determined from crystals grown in the presence of 4-O-benzyl-KdoOMe, 4-O-ethoxymethyl-KdoOMe, or 4-O-methoxymethyl-KdoOMe which, although unambiguous electron density corresponding to these antigens is not observed, revealed a number of novel CDR H3

conformations (Fig. 2). One structure (S25–39 Unliganded #3; crystallized in the presence of 4-O-ethoxymethyl-KdoOMe) shows broken electron density in the combining site that could accommodate the synthetic ligand 4-O-ethoxymethyl-KdoOMe (Fig. S13), which may indicate that the presence of weakly interacting molecules can alter the conformational equilibrium sufficiently to allow the crystallization of conformations that otherwise may be rare.

CDR H3 loops exist as conformational ensembles

The six new crystal structures presented here together with five reported previously (25, 27) comprise 20 crystallographically unique structures of the S25–2 and S25–39 Fabs (Table S3). Across these structures, the CDRs H1, H2, L2, and L3 maintain similar conformations and positions, CDR L1 maintains its conformation but varies in position relative to the binding site by as much as 4.2 Å, and CDR H3 adopts a
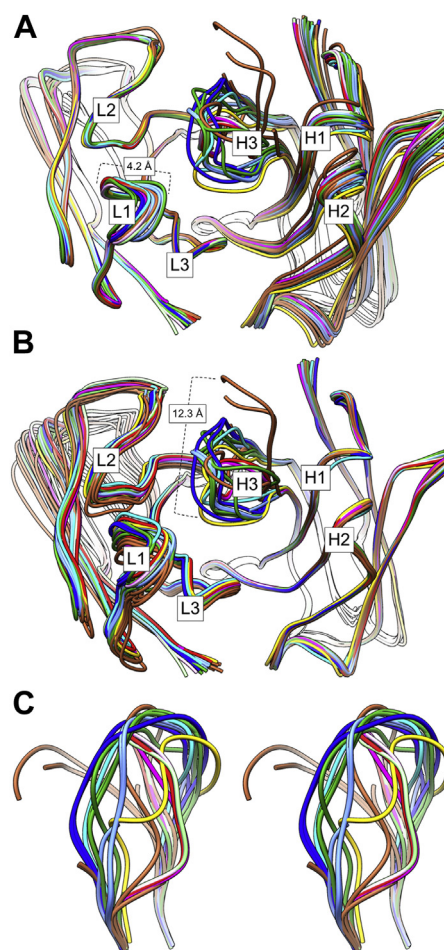

Figure 2. Conformational diversity of S25–2 and S25–39. A–C, the structures of all 20 crystallographically unique Fabs of S25–2 and S25–39 are shown superimposed by either (A) the VL domain or (B) the VH domain, and a stereo view of CDR H3 is shown in (C). The maximum displacement in CDR L1 was measured between Arg L27F Cα of 252_U3c and 252_U3d, and that of CDR H3 was measured between Glu H100A Cα of 2539_U3c and 2539_K. 252_K, light green; S252_U1, cyan; S252_U2, dark blue; 252_U3, dark green; 252_U4, light blue; 2539_K, magenta; 2539_4K, light pink; 2539_U1, yellow; 2539_U2, red; 2539_U3, brown. Shorthand labels are elaborated in Table S3. CDR, complementarity-determining region.

---

* A 'kinked' CDR H3 is defined by a pseudo-dihedral angle θ_{base} between $-100°$ and $100°$ from the Cα atoms of residues (n − 2) to (n + 1), where n is Kabat-numbered residue H102. An "extended" CDR H3 is defined by θ_{base} outside $-100°$ and $100°$.

◈ASBMB

J. Biol. Chem. (2022) 298(5) 101901 **3**

remarkable variety of conformations (Fig. 2). The 20 CDR H3 conformations fall into 8 clusters that differ by at least 1-Å Cα rmsd (Figs. 3 and S15), where the largest Cα rmsd between any two conformations is 6.5 Å, and the largest linear displacement of Cα atoms is 12.3 Å. This significant diversity generates multiple unique paratopes (Fig. 4) that reveal enhanced antigen binding capacities of S25−2 and S25−39.

Out of the eight conformational clusters of the S25−2 and S25−39 CDR H3 loops, 6 clusters (17 structures) contain conformations that are supported fully by electron density, while 2 clusters (3 structures) contain partial conformations with incomplete electron density in some portions of the H3 loops (Fig. S2). In the latter case, between one and four residues out of the 11 in the H3 loop were disordered. The fully defined conformations may represent those that lie in shallow free-energy minima, while the incomplete loops may indicate the presence of multiple relatively stable "partial conformations" with similar free energy. This variety of conformations with some measure of thermodynamic stability illustrates a "moderately rugged energy landscape" of protein conformations in equilibrium (30).

This is also apparent through comparison against the PyIgClassify database (31), where the S25−2 and S25−39 H3 loops can be classified into four distinct clusters (Table S5). These CDR structures, however, differ internally by as much as 40° or more from the cluster centroid, indicating that cluster assignment *via* this method may not provide a sufficiently nuanced comparison. Nevertheless, this analysis does emphasize the conformational variability present in the H3 loops of these antibody fragments.

Flexibility increases germline recognition potential

There is no structurally characterized precedent for the number of distinct paratopes displayed by the related near-germline antibodies S25−2 and S25−39, and with it the concomitant implications for polyspecificity. Reported polyspecificity in antibodies SPE7 (8), 7G12 (32), DNA-1 (33), and bH1 (7) occurs by the recognition of unique classes of antigen through a single or at most two different binding site conformations. The eight conformational clusters of the S25−2 and S25−39 CDR H3 loops, which very likely represent only a subset of the full conformational repertoires of these antibodies, reveal an astounding variety of unique paratopes that can be accessible through a single sequence to expand recognition potential.

The potential for polyspecificity through alternate conformations is foreshadowed further by S25−2 structures Unliganded #3 and #4, where the C-terminal tails of symmetry-related molecules are observed to form extensive interactions in the antibody-binding sites, including a salt bridge between Arg H52 and the symmetry-related Glu L213 that mimics the salt bridge formed to Kdo antigens. Similar interactions between the binding sites and the C-terminal tails of neighboring crystal mates have been observed for multiple other antibodies, with CDR H3 conformations different from those used to bind the antibodies' primary antigens (18).

With growing structural evidence for antibody polyspecificity through multiple binding site conformations, together with well-established evidence for germline antibody polyspecificity that decreases with affinity maturation (20, 21, 34−37), it is clear that some germline genes have evolved so that a single sequence can generate multiple unique paratopes
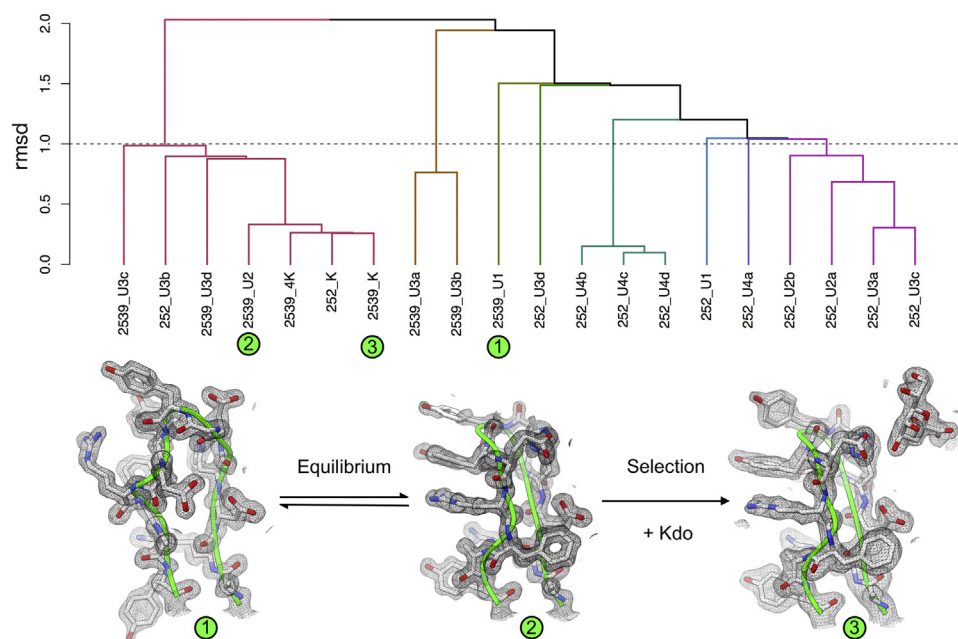

Figure 3. Conformational selection of S25−2 and S25−39 CDR H3. Single-linkage hierarchical clustering by Cα rmsd of all 20 crystallographically unique CDR H3 loops of S25−2 and S25−39 (61). Below the dendrogram, CDR H3s from selected S25−39 structures that summarize antigen binding by conformational selection are shown with 1σ 2Fo-Fc electron density maps. Separate dendrograms for S25−2 and S25−39 are provided in Fig. S15, and the Cα rmsd distance matrix is provided in Table S4. A heat map representations of the values in Table S4 is provided in Fig. S16. CDR, complementarity-determining region.
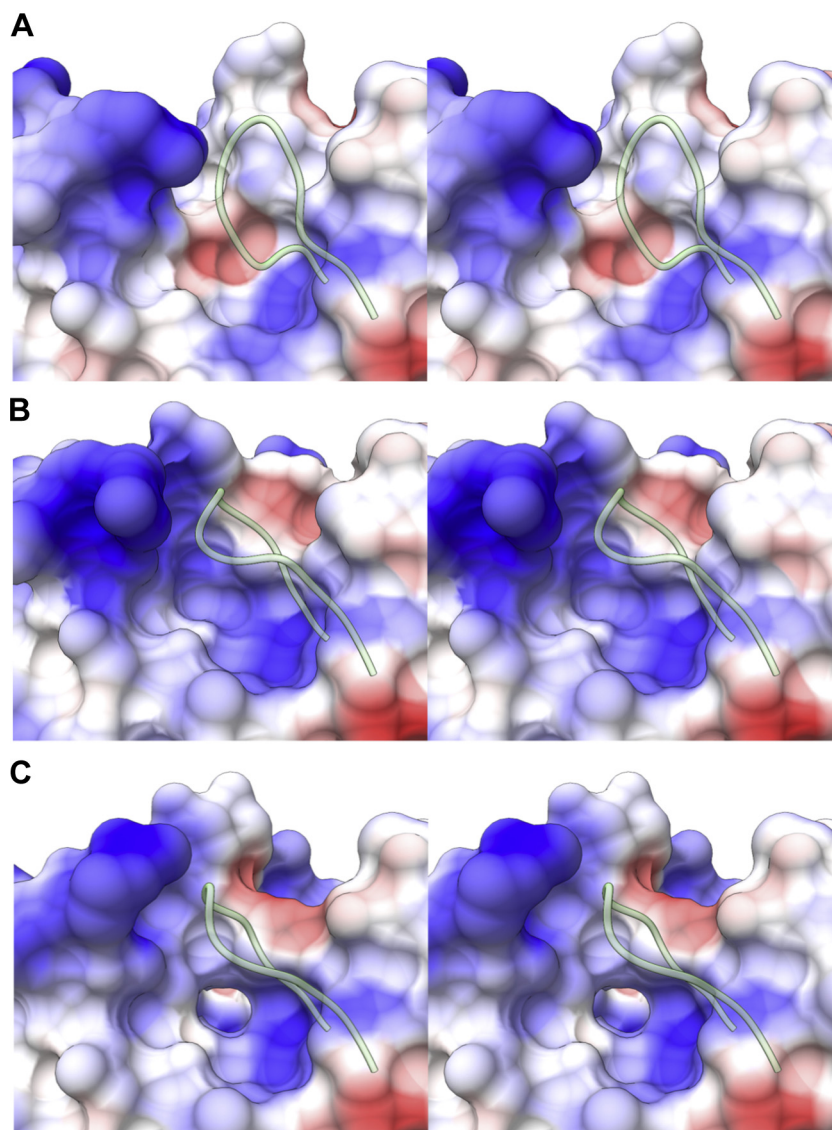
Figure 4. Paratope diversity of S25−2 and S25−39. *A–C*, electrostatic potential surfaces of paratopes from (A) 252_K, (B) 252_U1, and (C) 252_U3a, with CDR H3 overlaid in green, are shown to demonstrate the diversity generated from alternate CDR H3 conformations. Surfaces from all Fabs are provided in Fig. S17).

and amplify the recognition potential encoded by a limited germline.

S25−2 and S25−39 bind antigen through conformational selection

One of the well-ordered unliganded conformations of S25−39 is observed to be almost identical to the Kdo-bound conformation of both antibodies (Fig. 3). Together, these structures illustrate a conformational selection mechanism of ligand binding where an appropriate Kdo-based antigen selects the complementary CDR H3 conformation from equilibrium. The observation of the exact antigen-binding conformation in the absence of ligand supports the corollary that at least some of the other unliganded conformations are also the result of evolutionary pressure with distinct biological relevance rather than artifacts of crystal packing (9, 25).

The polyspecific antibodies SPE7 (8), 7G12 (32), DNA-1 (33), and bH1 (7) described earlier were each observed in one or two different bound conformations that are different from observed unliganded conformations and therefore do not demonstrate unambiguous CS. Hapten binding by SPE7 was shown to involve selection of a low-affinity isomer followed by IF to generate the final complex, illustrating a hybrid mechanism of selection and adjustment steps (8, 38). Polyspecificity of the antibody DNA-1 for ssDNA and HEPES through alternate CDR H3 conformations was suggested to occur through CS, but CDR H3 is disordered in unliganded structures, and it is therefore not possible to distinguish between IF and CS (6, 33). In contrast, the conformational selection illustrated by S25−39 is unambiguous: there is no evidence of CS followed by IF adjustment, as the exact liganded conformation is observed with clear electron density in the absence of ligand (Fig. 3). Our results are consistent with recent studies

⧜ASBMB

J. Biol. Chem. (2022) 298(5) 101901 **5**

that used metadynamics and molecular dynamics simulations to predict conformational ensembles of CDR H3 loops of several antibodies and found the crystallographically observed antigen-binding conformations in the absence of antigen in all cases, in addition to other crystallographically observed unliganded states (18, 20).

The presence of appropriate antigen-binding conformations existing in equilibrium may also reflect a significant general feature of anticarbohydrate antibodies. While germline antibodies responding to T-cell-dependent antigens (*e.g.*, proteins) are uniformly optimized through affinity maturation, those responding to T-cell-independent antigens (*e.g.*, most carbohydrates) generally are not (39), suggesting that the recognition of important carbohydrates (*i.e.*, from pathogens with which the immune system has coevolved) has been optimized in the germline (25). Maintenance of optimized carbohydrate binding together with a significant degree of polyspecificity *via* alternate CDR conformations would require the evolution of a conformational equilibrium between a discrete number of stable conformers that would allow antigen binding with low entropic penalties.

Cofactors expand germline recognition potential

The flexibility of the S25−2 CDR H3 is highlighted by the Unliganded #4 structure that displays a unique CDR H3 conformation with three coordinated iodide ions, including one at the base of CDR H3 that would require a significant opening of the binding site for its access (Fig. S14). Ion coordination may stabilize otherwise unfavorable conformations from equilibrium and increase potential for polyspecificity *via* the resulting paratopes. Indeed, iodide-influenced antibody paratopes have been shown to retain activity (40), multiple Ca^{2+}-dependent antibodies have been characterized (41–43), and several studies have shown that exposing pools of IgG to Fe^{2+} or heme greatly expand antibody polyreactivity (35, 44–47). The ability of an antibody to utilize cofactors to bind unique antigens, either by direct cofactor–antigen contact or by cofactor stabilization of otherwise unfavorable conformations, represents an even further expansion of antibody recognition potential beyond that available through sequence and conformational diversity.

Fv environment effects CDR H3 conformational equilibrium

S25−2 and S25−39 have only 10-amino acid differences between them, with four in each of the light and heavy chain V-gene framework regions, one at the tip of CDR H2, and one at position H101 encoded by the J gene at the base of CDR H3 (Table S1 and Fig. S18). Although the two antibodies utilize nearly identical CDR H3 conformations to bind Kdo antigens, they have not been observed in any of the same unliganded conformations. In the Kdo-bound conformation, Ser H101 of S25−2 makes hydrogen bonds to Arg H94 and Arg H100B within CDR H3 that the germline Ala H101 of S25−39 does not (Table S1 and Fig. S19). In several unliganded conformations, Ser H101 of S25−2 makes van der Waals contacts and/or hydrogen bonds with the light chain that Ala H101 of S25−39

does not. This single amino acid difference in CDR H3, together with potential long-range effects (between ∼9 and 30 Å) of the other nine amino acid differences in the Fv, evidently alters the conformational equilibria of these antibodies so that they are observed in different unliganded conformations in crystals. The sensitivity of S25−2 and S25−39 CDR H3 conformations to subtle differences in their environments further suggests that an identical CDR H3 paired with different germline V-gene combinations would yield significantly different conformational repertoires, which has major implications in antibody structure prediction and engineering (23, 31, 48–54).

Finally, despite S25−2 possessing the minor mutation away from germline in CDR H3, it is S25−39 (with the larger number of mutations distal to CDR H3) that was observed in the liganded conformation in the absence of ligand. It has been shown that the mutations in affinity-matured antibodies generally serve to make CDR H3 more rigid than their germline counterparts (18, 20, 21, 36, 37). It is possible that the different and additional mutations of S25−39 compared to S25−2 reduce its conformational diversity and increase the relative stability of the Kdo–antigen binding conformation so that it could be crystallized more readily in the absence of antigen.

Conclusions

The structures of related near-germline antibodies S25−2 and S25−39 reveal binding sites that not only are cross-reactive for multiple Kdo-based antigens through a single conformation but also exist in an equilibrium of significantly different conformations that generate unique paratopes that would allow for polyspecific recognition of unique antigens. Together, these mechanisms would enable a single germline antibody to protect against a large region of antigenic space and reconcile the limited size of the germline antibody repertoire with a near-limitless diversity of antigens in the environment. Significantly, the resulting new structures of S25−2 and S25−39 reveal an unprecedented level of conformational diversity in their combining sites and suggest a conformational selection mechanism of antigen binding with the exact antigen binding conformation observed as one among many unbound conformations.

When considering the generally accepted difficulty in crystallizing proteins with flexible segments, this study provides the first direct observation of the remarkable flexibility necessary to enable antigen binding through conformational selection. Such a mechanism allows the germline repertoire to maintain recognition of evolutionarily important antigens while remaining adaptable to new threats through the presentation of a range of stable conformations.

Experimental procedures
Antibody production

S25−2 and S25−39 IgG and Fab were produced and purified as described previously (26, 27).

Synthesis of 4-O-modified Kdo ligands

See supporting information.

Crystallization of S25–39 and S25–2 Fab

S25–39 and S25–2 Fab were crystallized in the presence of synthetic ligands 4-O-methyl-KdoOAll, 4-O-benzyl-KdoOMe, 4-O-ethoxymethyl-KdoOMe, and 4-O-methoxymethyl-KdoOMe, each with 12 mg/ml Fab (in 20 mM Hepes, pH 7.5) and 5 mM ligand (in 20 mM Hepes, pH 7.5), using Hampton Crystal Screen 1 and 2 in hanging-drop vapor diffusion plates set up by hand at 1:1 ratios of protein to reservoir solution and using Qiagen Pegs I and Pegs II screens in 96-well sitting-drop Intelli-plates set up with an ARI Crystal Gryphon robot at 1:1 and 2:1 protein-to-reservoir ratios. Initial hits were optimized in 35 × 10-mm tissue culture plates by hanging-drop vapor diffusion. The conditions yielding the final crystals from which structures were solved were as follows: S25–2 Unliganded #3: 0.2 M ammonium fluoride, 20% PEG 3350, 5 mM 4-O-methoxymethyl-KdoOMe; S25–2 Unliganded #4: 0.2 M ammonium iodide, 20% PEG 3350, 5 mM 4-O-methoxymethyl-KdoOMe; S25–39 with 4-O-methyl-KdoOAll: 0.1 M Hepes, pH 7.0, 30% Jeffamine ED-2001, 5 mM 4-O-methyl-KdoOAll; S25–39 Unliganded #1: 0.1 M bis-Tris, pH 6.5, 20% PEG MME 2000, 5 mM 4-O-methoxymethyl-KdoOMe; S25–39 Unliganded #2: 0.15 M potassium bromide, 30% PEG MME 2000, 5 mM 4-O-methoxymethyl-KdoOMe; S25–39 Unliganded #3: 0.1 M sodium Hepes, pH 7.5, 25% PEG MME 2000, 5 mM 4-O-ethoxymethyl-KdoOMe.

Data collection, structure determination, and refinement

Before freezing, crystals were dipped in reservoir solution with the addition of 30% MPD for cryoprotection. Crystals were flash-frozen to −160 °C using an Oxford Cryostream 700 crystal cooler (Oxford Cryosystems). Data were collected either on a Rigaku R-AXIS 4++ area detector with X-rays produced by a Rigaku MM-003 generator or on beamline CMCF-ID at the Canadian Light Source synchrotron. The data were scaled, averaged, and integrated using HKL2000 (55). Structures were solved by molecular replacement using Phaser (56), with previously solved structures of S25–2 (1Q9K) or S25–39 (3OKD) as search models. Model building was carried out with Coot (57) and SetoRibbon (Evans, unpublished). Refinement was carried out using Refmac5 (58) through the CCP4i interface (59). Final model and refinement statistics are given in Table S2.

Figures

All structural figures were created using UCSF Chimera (60). Chimera is developed by the Resource for Biocomputing, Visualization, and Informatics at the University of California, San Francisco (supported by NIGMS P41-GM103311). Dendrograms were created using the single-linkage hierarchical clustering method of *hclust* in R (61).

Data availability

The atomic coordinates and structure factors (Table S2) have been deposited in the Protein Data Bank, Research Collaboratory for Structural Bioinformatics, Rutgers University, New Brunswick, NJ (http://www.rcsb.org/).

References

1. Maizels, N. (2005) Immunoglobulin gene diversification. *Annu. Rev. Genet.* **39**, 23–46
2. Georgiou, G., Ippolito, G. C., Beausang, J., Busse, C. E., Wardemann, H., and Quake, S. R. (2014) The promise and challenge of high-throughput sequencing of the antibody repertoire. *Nat. Biotechnol.* **32**, 158–168
3. Richards, F. F., Konigsberg, W. H., Rosenstein, R. W., and Varga, J. M. (1975) On the specificity of antibodies. *Science* **187**, 130–137
4. Van Regenmortel, M. H. V. (2014) Specificity, polyspecificity, and hetero-specificity of antibody-antigen recognition. *J. Mol. Recognit.* **27**, 627–639
5. Khan, T., and Salunke, D. M. (2014) Adjustable locks and flexible keys: Plasticity of epitope-paratope interactions in germline antibodies. *J. Immunol.* **192**, 5398–5405
6. Schuermann, J. P., Prewitt, S. P., Davies, C., Deutscher, S. L., and Tanner, J. J. (2005) Evidence for structural plasticity of heavy chain complementarity-determining region 3 in antibody-ssDNA recognition. *J. Mol. Biol.* **347**, 965–978
7. Bostrom, J., Yu, S.-F., Kan, D., Appleton, B. A., Lee, C. V., Billeci, K., Man, W., Peale, F., Ross, S., Wiesmann, C., and Fuh, G. (2009) Variants of the antibody herceptin that interact with HER2 and VEGF at the antigen binding site. *Science* **323**, 1610–1614
8. James, L. C., Roversi, P., and Tawfik, D. S. (2003) Antibody multi-specificity mediated by conformational diversity. *Science* **299**, 1362–1367
9. Schulze-Gahmen, U., Rini, J., and Wilson, I. (1993) Detailed analysis of the free and bound conformations of an antibody; X-ray structures of fab 17/9 and three different fab-peptide complexes. *J. Mol. Biol.* **234**, 1098–1118
10. Vogt, A. D., Pozzi, N., Chen, Z., and Di Cera, E. (2014) Essential role of conformational selection in ligand binding. *Biophysical Chem.* **186**, 13–21
11. Weikl, T. R., and Paul, F. (2014) Conformational selection in protein binding and function. *Protein Sci.* **23**, 1508–1518
12. Rini, J. M., Schulze-Gahmen, U., and Wilson, I. A. (1992) Structural evidence for induced fit as a mechanism for antibody-antigen recognition. *Science* **255**, 959–965

13. Dimitrov, J. D., Pashov, A. D., and Vassilev, T. L. (2012) Antibody polyspecificity: What does it matter? *Adv. Exp. Med. Biol.* **750**, 213–226
14. Wang, W., Ye, W., Yu, Q., Jiang, C., Zhang, J., Luo, R., and Chen, H. F. (2013) Conformational selection and induced fit in specific antibody and antigen recognition: SPE7 as a case study. *J. Phys. Chem. B* **117**, 4912–4923
15. Manivel, V., Bayiroglu, F., Siddiqui, Z., Salunke, D. M., and Rao, K. V. S. (2002) The primary antibody repertoire represents a linked network of degenerate antigen specificities. *J. Immunol.* **169**, 888–897
16. Jimenez, R., Salazar, G., Baldridge, K. K., and Romesberg, F. E. (2003) Flexibility and molecular recognition in the immune system. *Proc. Natl. Acad. Sci. U. S. A.* **100**, 92–97
17. Foote, J., and Milstein, C. (1994) Conformational isomerism and the diversity of antibodies. *Proc. Natl. Acad. Sci. U. S. A.* **91**, 10370–10374
18. Fernández-Quintero, M. L., Kraml, J., Georges, G., and Liedl, K. R. (2019) CDR-H3 loop ensemble in solution – conformational selection upon antibody binding. *mAbs* **11**, 1077–1088
19. Kaur, H., Sain, N., Mohanty, D., and Salunke, D. M. (2018) Deciphering evolution of immune recognition in antibodies. *BMC Struct. Biol.* **18**, 19
20. Fernández-Quintero, M. L., Loeffler, J. R., Kraml, J., Kahler, U., Kamenik, A. S., and Liedl, K. R. (2019) Characterizing the diversity of the CDR-H3 loop conformational ensembles in relationship to antibody binding properties. *Front. Immunol.* **9**, 3065
21. Adhikary, R., Yu, W., Oda, M., Walker, R. C., Chen, T., Stanfield, R. L., Wilson, I.a., Zimmermann, J., and Romesberg, F. E. (2015) Adaptive mutations alter antibody structure and dynamics during affinity maturation. *Biochemistry* **54**, 2085–2093
22. Lang, K. S., Burow, A., Kurrer, M., Lang, P. A., and Recher, M. (2007) The role of the innate immune response in autoimmune disease. *J. Autoimmun.* **29**, 206–212
23. Marks, C., and Deane, C. M. (2017) Antibody H3 structure prediction. *Comput. Struct. Biotechnol. J.* **15**, 222–231
24. Blackler, R. J., Müller-Loennies, S., Brade, L., Kosma, P., Brade, H., and Evans, S. V. (2012) Antibody recognition of Chlamydia LPS: Structural insights of inherited immune responses. In: Kosma, P., Müller-Loennies, S., eds. *Anticarbohydrate Antibodies*, Springer Vienna, Vienna: 75–120
25. Nguyen, H. P., Seto, N. O. L., MacKenzie, C. R., Brade, L., Kosma, P., Brade, H., and Evans, S. V. (2003) Germline antibody recognition of distinct carbohydrate epitopes. *Nat. Struct. Biol.* **10**, 1019–1025
26. Brooks, C. L., Müller-Loennies, S., Brade, L., Kosma, P., Hirama, T., MacKenzie, C. R., Brade, H., and Evans, S. V. (2008) Exploration of specificity in germline monoclonal antibody recognition of a range of natural and synthetic epitopes. *J. Mol. Biol.* **377**, 450–468
27. Blackler, R. J., Müller-Loennies, S., Brooks, C. L., Evans, D. W., Brade, L., Kosma, P., Brade, H., and Evans, S. V. (2011) A common NH53K mutation in the combining site of antibodies raised against chlamydial LPS glycoconjugates significantly increases avidity. *Biochemistry* **50**, 3357–3368
28. Abhinandan, K. R., and Martin, A. C. R. (2008) Analysis and improvements to Kabat and structurally correct numbering of antibody variable domains. *Mol. Immunol.* **45**, 3832–3839
29. Kuroda, D., Shirai, H., Kobori, M., and Nakamura, H. (2008) Structural classification of CDR-H3 revisited: A lesson in antibody modeling. *Proteins* **73**, 608–620
30. James, L. C., and Tawfik, D. S. (2003) Conformational diversity and protein evolution – a 60-year-old hypothesis revisited. *Trends Biochem. Sci.* **28**, 361–368
31. North, B., Lehmann, A., and Dunbrack, R. L. (2011) A new clustering of antibody CDR loop conformations. *J. Mol. Biol.* **406**, 228–256
32. Yin, J., Beuscher, A. E., Andryski, S. E., Stevens, R. C., and Schultz, P. G. (2003) Structural plasticity and the evolution of antibody affinity and specificity. *J. Mol. Biol.* **330**, 651–656
33. Schuermann, J. P., Henzl, M. T., Deutscher, S. L., and Tanner, J. J. (2004) Structure of an anti-DNA fab complexed with a non-DNA ligand provides insights into cross-reactivity and molecular mimicry. *Proteins* **57**, 269–278
34. Shehata, L., Maurer, D. P., Wec, A. Z., Lilov, A., Champney, E., Sun, T., Archambault, K., Burnina, I., Lynaugh, H., Zhi, X., Xu, Y., and Walker, L. M. (2019) Affinity maturation enhances antibody specificity but compromises conformational stability. *Cell Rep.* **28**, 3300–3308.e4
35. Kanyavuz, A., Marey-Jarossay, A., Lacroix-Desmazes, S., and Dimitrov, J. D. (2019) Breaking the law: Unconventional strategies for antibody diversification. *Nat. Rev. Immunol.* **19**, 355–368
36. Xu, H., Schmidt, A. G., O'Donnell, T., Therkelsen, M. D., Kepler, T. B., Moody, M. A., Haynes, B. F., Liao, H., Harrison, S. C., and Shaw, D. E. (2015) Key mutations stabilize antigen-binding conformation during affinity maturation of a broadly neutralizing influenza antibody lineage. *Proteins* **83**, 771–780
37. Li, T., Tracka, M. B., Uddin, S., Casas-Finet, J., Jacobs, D. J., and Livesay, D. R. (2015) Rigidity emerges during antibody evolution in three distinct antibody systems: Evidence from QSFR analysis of fab fragments. *PLoS Comput. Biol.* **11**, e1004327
38. James, L. C., and Tawfik, D. S. (2005) Structure and kinetics of a transient antibody binding intermediate reveal a kinetic discrimination mechanism in antigen recognition. *Proc. Natl. Acad. Sci. U. S. A.* **102**, 12730–12735
39. Fairfax, K. A., Kallies, A., Nutt, S. L., and Tarlinton, D. M. (2008) Plasma cell development: From B-cell subsets to long-term survival niches. *Semin. Immunol.* **20**, 49–58
40. Golinelli-Pimpaneau, B., Luthi, C., and Christen, P. (2006) Structural basis for D-amino acid transamination by the pyridoxal 5′-Phosphate-dependent catalytic antibody 15A9. *J. Biol. Chem.* **281**, 23969–23977
41. Wojciak, J. M., Zhu, N., Schuerenberg, K. T., Moreno, K., Shestowsky, W. S., Hiraiwa, M., Sabbadini, R., and Huxford, T. (2009) The crystal structure of sphingosine-1-phosphate in complex with a Fab fragment reveals metal bridging of an antibody and its antigen. *Proc. Natl. Acad. Sci. U. S. A.* **106**, 17717–17722
42. Zhou, T., Hamer, D. H., Hendrickson, W. A., Sattentau, Q. J., and Kwong, P. D. (2005) Interfacial metal and antibody recognition. *Proc. Natl. Acad. Sci. U. S. A.* **102**, 14575–14580
43. Stearns, D. J., Kurosawa, S., Sims, P. J., Esmon, N. L., and Esmon, C. T. (1988) The interaction of a Ca^{2+}-dependent monoclonal antibody with the protein C activation peptide region. Evidence for obligatory $Ca2^+$ binding to both antigen and antibody. *J. Biol. Chem.* **263**, 826–832
44. McIntyre, J. A., and Faulk, W. P. (2009) Redox-reactive autoantibodies: Biochemistry, characterization, and specificities. *Clin. Rev. Allergy Immunol.* **37**, 49–54
45. Dimitrov, J. D., Roumenina, L. T., Doltchinkova, V. R., Mihaylova, N. M., Lacroix-Desmazes, S., Kaveri, S. V., and Vassilev, T. L. (2007) Antibodies use heme as a cofactor to extend their pathogen elimination activity and to acquire new effector functions. *J. Biol. Chem.* **282**, 26696–26706
46. Gupta, N., de Wispelaere, M., Lecerf, M., Kalia, M., Scheel, T., Vrati, S., Berek, C., Kaveri, S. V., Desprès, P., Lacroix-Desmazes, S., and Dimitrov, J. D. (2015) Neutralization of Japanese Encephalitis virus by heme-induced broadly reactive human monoclonal antibody. *Sci. Rep.* **5**, 16248
47. Dimitrov, J. D., Ivanovska, N. D., Lacroix-Desmazes, S., Doltchinkova, V. R., Kaveri, S. V., and Vassilev, T. L. (2006) Ferrous ions and reactive oxygen species increase antigen-binding and anti-inflammatory activities of immunoglobulin G. *J. Biol. Chem.* **281**, 439–446
48. Weitzner, B. D., Jeliazkov, J. R., Lyskov, S., Marze, N., Kuroda, D., Frick, R., Adolf-Bryfogle, J., Biswas, N., Dunbrack, R. L., and Gray, J. J. (2017) Modeling and docking of antibody structures with Rosetta. *Nat. Protoc.* **12**, 401–416
49. Almagro, J. C., Teplyakov, A., Luo, J., Sweet, R. W., Kodangattil, S., Hernandez-Guzman, F., and Gilliland, G. L. (2014) Second antibody modeling assessment (AMA-II): 3D antibody modeling. *Proteins* **82**, 1553–1562
50. Almagro, J. C., Beavers, M. P., Hernandez-Guzman, F., Maier, J., Shaulsky, J., Butenhof, K., Labute, P., Thorsteinson, N., Kelly, K., Teplyakov, A., Luo, J., Sweet, R., and Gilliland, G. L. (2011) Antibody modeling assessment. *Proteins* **79**, 3050–3066
51. Dunbar, J., Krawczyk, K., Leem, J., Marks, C., Nowak, J., Regep, C., Georges, G., Kelm, S., Popovic, B., and Deane, C. M. (2016) SAbPred: A structure-based antibody prediction server. *Nucleic Acids Res.* **44**, W474–W478
52. Leem, J., Dunbar, J., Georges, G., Shi, J., and Deane, C. M. (2016) ABodyBuilder: Automated antibody structure prediction with data–driven accuracy estimation. *MAbs* **8**, 1259–1268
53. Lepore, R., Olimpieri, P. P., Messih, M. A., and Tramontano, A. (2017) PIGSPro: Prediction of immunoGlobulin structures v2. *Nucleic Acids Res.* **45**, W17–W23

54. Weitzner, B. D., and Gray, J. J. (2017) Accurate structure prediction of CDR H3 loops enabled by a novel structure-based C-terminal constraint. *J. Immunol.* **198**, 505–515

55. Otwinowski, Z., and Minor, W. (1997) Processing of X-ray diffraction data collected in oscillation mode. *Methods Enzymol.* **276**, 307–326

56. McCoy, A. J., Grosse-Kunstleve, R. W., Adams, P. D., Winn, M. D., Storoni, L. C., and Read, R. J. (2007) Phaser crystallographic software. *J. Appl. Crystallogr.* **40**, 658–674

57. Emsley, P., Lohkamp, B., Scott, W. G., and Cowtan, K. (2010) Features and development of coot. *Acta Crystallogr. D. Biol. Crystallogr.* **66**, 486–501

58. Murshudov, G. N., Skubák, P., Lebedev, A. A., Pannu, N. S., Steiner, R. a, Nicholls, R. a, Winn, M. D., Long, F., and Vagin, A. A. (2011) REFMAC5 for the refinement of macromolecular crystal structures. *Acta Crystallogr. D. Biol. Crystallogr.* **67**, 355–367

59. Winn, M. D., Ballard, C. C., Cowtan, K. D., Dodson, E. J., Emsley, P., Evans, P. R., Keegan, R. M., Krissinel, E. B., Leslie, A. G. W., McCoy, A., McNicholas, S. J., Murshudov, G. N., Pannu, N. S., Potterton, E. A., Powell, H. R., *et al.* (2011) Overview of the CCP4 suite and current developments. *Acta Crystallogr. D. Biol. Crystallogr.* **67**, 235–242

60. Pettersen, E. F., Goddard, T. D., Huang, C. C., Couch, G. S., Greenblatt, D. M., Meng, E. C., and Ferrin, T. E. (2004) UCSF Chimera - a visualization system for exploratory research and analysis. *J. Comput. Chem.* **25**, 1605–1612

61. R Core Team (2017) *R: A Language and Environment for Statistical Computing.*, R Foundation for Statistical Computing, Vienna, Austria

Ryan J. Blackler received his PhD in Biochemistry from the University of Victoria, where he utilized X-ray crystallography to study the structural basis of antibody cross-reactivity and polyspecificity, as culminated in this article. He is now pursuing a career as a protein engineer, where he applies the experience gained during his doctoral studies towards the research and development of multi-specific antibodies and other novel fusion proteins for therapeutic applications. www.linkedin.com/in/ryan-blackler.